Nonlinear Hyperspectral Unmixing Using Nonlinearity Order Estimation and Polytope Decomposition

Andrea Marinoni, *Member, IEEE*, Javier Plaza, *Member, IEEE*, Antonio Plaza, *Fellow, IEEE*, and Paolo Gamba, *Fellow, IEEE*

***Abstract*—Nonlinear hyperspectral unmixing (HSU) plays a key-role in understanding and quantifying the physical-chemical phenomena occurring over geometrically complex fields of view. Nonlinear HSU methods that do not rely on prior knowledge of the ground truth to analyze the scene are especially interesting. However, they can be affected either by overfitting or performance degradation provided by inaccurate setting of unmixing parameters. In this paper, we introduce a new nonlinear HSU architecture which aims at taking advantage of the benefit provided by the combination of polytope decomposition (POD) method together with artificial neural network (ANN)-based learning. Specifically, ANN is able to efficiently estimate the order p of the nonlinearity provided by the given scene even without the thorough knowledge of the ground truth. The ANN-based learning is used to feed the POD in order to deliver accurate unmixing based on a p-linear polynomial model. Experimental results over simulated and real scenes show promising performance of the proposed framework.**

***Index Terms*—Artificial neural network (ANN), linear programming, nonlinear hyperspectral unmixing (HSU), p-order polynomial models, polytope decomposition (POD).**

I. INTRODUCTION

RECENTLY, the analysis of human–environment interactions has become crucial for several social, financial, health and environmental research fields [1]. Indeed, deep knowledge of the anthropogenic impact on environment can help in investigating epidemiological flows, predicting population distribution and determining community policies to drive sustainable developments [2].

In order to thoroughly understand the characteristics and behavior of the aforementioned interactions, it is necessary to model, study, and classify the physical–chemical properties of a region (see for instance [3]). However, the collection of natural records s.t. this analysis can be performed is typically spatially limited. Therefore, the study of structural composition over geographic regions can take advantage of hyperspectral imagery, as it provides information with both high spectral and spatial resolution. In this regard, hyperspectral unmixing (HSU) represents one of the most powerful and remarkable tools for delivering effective analyses of the physical components in the instantaneous field of view.

HSU methods aim at separating the target pixel spectra into a set of constituent spectral signatures (*endmembers*) and a set of fractional *abundances*. Typically, endmembers are assumed to identify the pure materials in the given image, while abundances report the percentage of each endmember in a pixel. However, the definition of the aforementioned parameters changes according to the mixture model that is considered [4]. Specifically, mixing models can be classified in linear or nonlinear. Linear mixing models (LMMs) hold when incident light interacts at a macroscopic scale with just one material per pixel [5]. Several papers have addressed this topic in literature. LMMs are often employed in HSU as they are quite easy to implement. On the other hand, LMMs can hardly deliver efficient unmixing performance as more complex mixing phenomena occur [6].

NLMMs have been developed in order to improve the description of the macroscopic-scale interactions among the constituent materials. Polynomial functions can be applied to model the nonlinearities provided by layer partitions and scattering properties. Bilinear mixture models (BMMs) play a key role in this class of schemes [7], [8], since they are widely used in nonlinear HSU. Unsupervised methods have been developed to exploit the nonlinear effects, i.e., no ground truth information is needed in HSU process. Basically, they aim at characterizing the interactions that occur in a hyperspectral scene among couples of constituent materials. Thus, interferences among endmembers that occur at a higher order of nonlinearity are not described. Further, reflectance contributions which result from multiple scatterings among several endmembers are not properly characterized [9].

It is worth noting that higher order nonlinear contributions might be considered negligible in specific scenarios (see for instance [10]). On the other hand, when several endmembers of different nature get close over a given region, the energy provided by multiple scatterings and acquired by the sensor is not negligible at all. Fig. 1 reports three examples of scenarios that

Manuscript received July 30, 2014; revised March 27, 2015; accepted April 21, 2015. Date of publication May 14, 2015; date of current version July 30, 2015. This paper represents an enhanced version of A. Marinoni, J. Plaza, A. Plaza, P. Gamba, "Integrating multiple nonlinear estimators into hyperspectral unmixing," presented at IEEE WHISPERS 2014, Lausanne, Switzerland.

A. Marinoni and P. Gamba are with the Telecommunications and Remote Sensing Laboratory, Department of Electrical, Computer, and Biomedical Engineering, University of Pavia, I-27100 Pavia, Italy (e-mail: andrea.marinoni@unipv.it; paolo.gamba@unipv.it).

J. Plaza and A. Plaza are with the Hyperspectral Computing Laboratory, Department of Computer Technology and Communications, University of Extremadura, E-10071 Cáceres, Spain (e-mail: jplaza@unex.es; aplaza@unex.es).

Color versions of one or more of the figures in this paper are available online at http://ieeexplore.ieee.org.

Digital Object Identifier 10.1109/JSTARS.2015.2427517

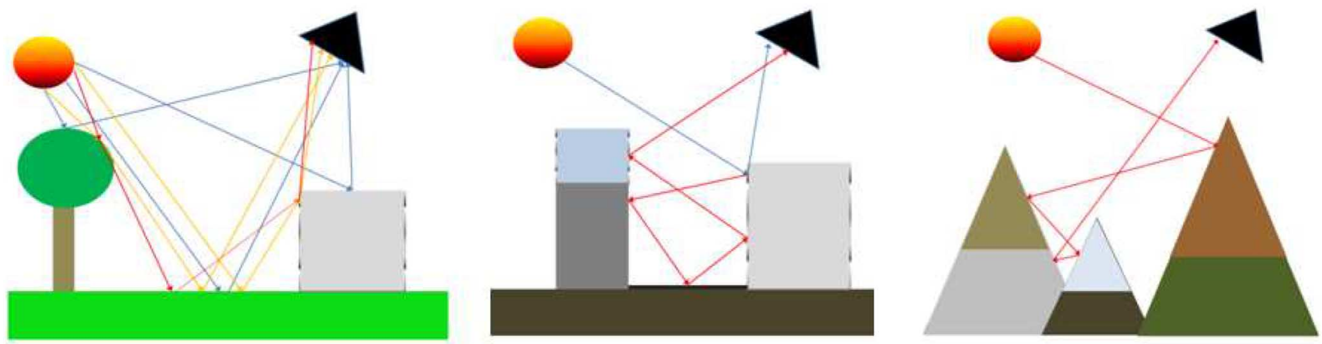

(a) (b) (c)

Fig. 1. Schemes of geometrically complex scenes where the higher order nonlinear contributions provided by multiple scatterings are not negligible: (a) three endmembers scenario; (b) instance of urban scenario; (c) instance of multilayer scenario.

frequently occur when performing HSU. Specifically, Fig. 1(a) shows how three close endmembers can interact in delivering reflectance power to the sensor. LMM can characterize light blue contributions, while BMMs are able to describe light blue and orange contributions. However, LMMs and BMMs can not efficiently track the red patterns of the light, as it is delivered by the interaction of the endmembers that show up nearby in the considered scene.

This effect is even more emphasized in Fig. 1(b), where an instance of urban scenario is sketched. Indeed, when anthropogenic materials show up and interplay over an hyperspectral scene, absorption is so restrained that reflections can deliver relevant contributions to the sensor also after several reflectance interactions.

Finally, multilayer scenarios [sketched in Fig. 1(c)] deliver higher order reflectance inputs as well. In fact, as light has the possibility to interact with different endmembers at different depths, the reflectance recorded by the sensor is strongly affected by the interplay that occurs among the elements that show up over in-depth. Hence, Fig. 1(c) can be considered as a sketch of the reflectance interaction that shows up over a nonflat scenario at macroscopic scale (e.g., a hilly region or a mountain sample) or microscopic scale (e.g., a scene where several minerals show up). It is important to remind that the aforementioned multilayer interactions can occur also over water basins where in-depth elements (such as pollutants, residuals, or hydric flora) interplay to originate the spectral signal recorded by the sensor.

In [11], the authors introduce a new model that aims at involving all these effects in an order-p nonlinear polynomial scheme, where $p \geq 2$. This unsupervised method, which is based on polytope decomposition (POD), delivers very good HSU performance as the nonlinearity follows a polynomial behavior. On the other hand, if super-polynomial effects (e.g., sinusoidal) or microscopic-scale mixtures occur, POD cannot efficiently track the interaction characteristics. Therefore, more complex methods are required.

Indeed, as photonic interactions or multilayer mixtures show up, NLMMs that thoroughly describe the intimate mixtures of the constituent materials have been proposed [7]. These schemes (such as Hapke's model) result from theoretical analyses and aim at accurately tracing the reflectance behavior when considering a scene having specific geomorphical, chemical and physical properties. Hence, the aforesaid models require perfect knowledge of the geometric location of the given sensor. Supervised methods such as kernel-based and artificial neural networks (ANNs) have been proposed to perform unmixing on microscopic scale [4], [7]. These algorithms can track every nonlinearity behavior; however, as previously mentioned, they need reliable training samples to properly initiate the learning process.

Combining unsupervised and supervised methods in order to exploit only the advantages from the two classes of algorithms can help in efficiently perform nonlinear HSU, while minimizing at the same time the effect of the drawbacks of each scheme. Specifically, properly set architectures can drive excellent performance in nonlinear HSU improving the nonlinearity characterization without the constraint of prior knowledge of the ground scene.

In this work, we present a novel framework for nonlinear HSU which combines POD with ANN-based learning (Fig. 2). Previous studies [11] have shown that the POD method is able to deliver very good performance in terms of reconstruction error (RE) over scenes where no ground-truth is previously available and the nonlinearity can be described by means of polynomials. It has been observed, however, that if the nonlinearity is nonpolynomial, the POD method does not show good performance in HSU. Further, the aforementioned method cannot estimate the order of the nonlinearity itself, an aspect that can lead to lower unmixing performance and/or overfitting. These issues can be addressed by using supervised ANNs which are able to deliver unmixing performance for a wider range of nonlinearities. Even if no ground-truth information is available, the ANN can still efficiently estimate the order of the nonlinearity involved in the problem, thus enhancing the capacity of the POD method. Hence, it is possible to set up a framework for unsupervised HSU that makes use of the POD method in order to achieve the nonlinear coefficients and to efficiently reconstruct the image from the extracted endmembers.

This paper is organized as follows. Section II describes the POD and ANN methods used in this work to develop the proposed approach. Section III presents an experimental validation of the proposed approach. Section IV provides the final remarks and future research lines.

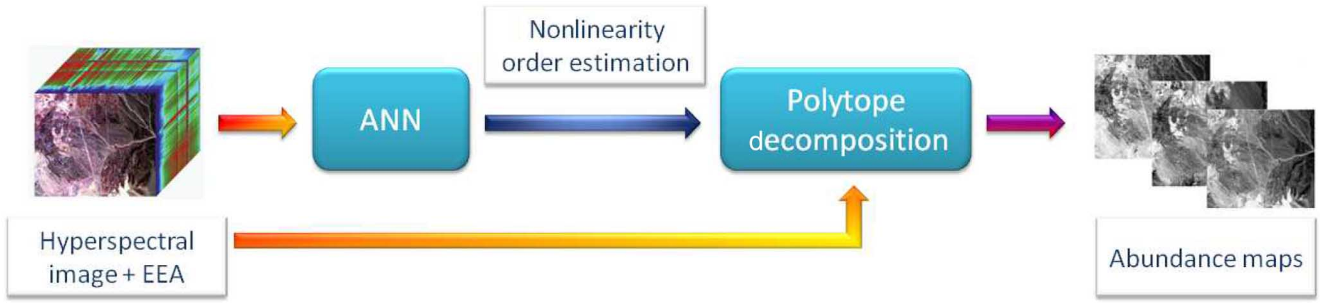

Fig. 2. Scheme of the proposed framework for nonlinear spectral unmixing.

II. Method

Fig. 2 shows a flowchart of the proposed approach, which is made up of the combination of POD and ANN techniques applied to the original hyperspectral image after obtaining a set of endmembers using an endmember extraction algorithm (EEA). In this section, we describe the aforementioned methods in more details.

A. Artificial Neural Network (ANN)

Although many neural network architectures exist, feedfordward networks have been widely used in the context spectral unmixing in terms of nonlinear relationships [12]–[14]. In this work, we adopt a multilayer perceptron (MLP) architecture which is easily adaptable to provide nonlinearity order estimations, due to its proved ability as nonlinear classifier.

The MLP is composed of an input layer, two hidden layers, and an output layer. The node count in the input layer is fixed to the spectral dimensionality of the data (number of spectral bands of the considered dataset). The number of output nodes equals the maximum number of possible orders to be estimated, thus, the target outputs of the network are vectors with as many components as possible orders to be estimated containing binary values in the set $\{-1, +1\}$. Output vectors will show a $+1$ at the correct order position and -1 everywhere else. Finally, logistic activation functions are used in both hidden layers, while hyperbolic tangent is implemented in the output layer.

In order to avoid overfitting and improve generalization, we decided to use sufficiently large hidden layers in combination with regularization techniques (instead of early-stopping or cross-validation techniques) which involve the modification of the performance function embedding a term that consists of the mean of the sum of squares of the network weights and biases. Particularly, we use the Bayesian regulation backpropagation training algorithm, which updates the weight and bias according to Levenberg–Marquard optimization algorithm, which is used to estimate the Hessian matrix of the performance function. Traditionally, feedforward networks use the mean square error, i.e., average square error between target outputs (t_i) and network outputs (y_i), as follows:

$$F = MSE = \frac{1}{\varnothing}\sum_{i=1}^{\varnothing}(e_i)^2 = \frac{1}{\varnothing}\sum_{i=1}^{\varnothing}(t_i - y_i)^2 \quad (1)$$

where $\varnothing$ is the number of output nodes of the network.

However, it is possible to improve generalization by modifying the performance function to enforce the network to have smaller weights and bias, thus smoothing the convergence reducing the probability of overfitting. The modified performance function is as follows:

$$\begin{aligned} F &= MSEREG \\ &= \gamma\left(\frac{1}{\varnothing}\sum_{i=1}^{\varnothing}(t_i - y_i)^2\right) + (1-\gamma)\left(\frac{1}{n}\sum_{i=1}^{n}(w_i)^2\right) \end{aligned} \quad (2)$$

where γ is an adaptive performance ratio used to determine the direction (minimal error or minimal weights) that the network must seek and $W = [w_i]_{i=1,\ldots,n}$ is a vector containing the whole set of weights and biases of the network.

Considering that the MLP is used to estimate the nonlinearity order of an image and due to the lack of available reference information for real images, we employ an innovative approach where, from the endmembers extracted by an EEA, we generate synthetic nonlinear combinations of their spectral signatures according to the model proposed in [11] using (7). Then, we use such nonlinear combinations to generate both training set (nonlinear combinations of endmembers) and test set (binary vectors) to be used during the ANN training stage. It should be noticed that we can generate infinite training and testing samples from an *a priori* estimated set of endmembers, being the range of possible nonlinearity orders the only needed parameter, thus reducing the impact of the curse of dimensionality [15]. However, the determination of optimal training sets is beyond the scope of this paper. In the experimental validation. we just show a proof of concept of how a set of randomly generated training samples is able to be efective in the context of nonlinearity order estimations. Additional experiments searching for best configurations, minimum training sets and optimal nonlinear estimators will be treated in future research lines.

B. Polytope Decomposition (POD)

Let $\underline{y}_l = [y_{l_n}]_{n=1,\ldots,N}$, $y_{l_n} \in \mathbb{R}$ be the N-band spectral signature of the lth pixel in a hyperspectral image. Let us assume that the signature $\underline{y}_l$ is a nonlinear combination of R endmembers $\underline{m}_r = [m_{r_n}]_{n=1,\ldots,N}$, being $r = 1, \ldots, R$. Hence, a polynomial model that aims at representing order-p nonlinear multiple scatterings and interferences provided by R endmembers over the lth pixel can be derived by properly setting the parameters and coefficients in the order-p mixing model, which can be analytically written as follows:

$$\begin{aligned}\underline{y}_l &= \sum_{r=1}^{R} a_{rl}\underline{m}_r \\ &+ \sum_{k=2}^{p}\left\{\sum_{i=1}^{\tau_1}\sum_{j=\tau_2}^{R}[\vartheta_{ikl}\underline{m}_i + \vartheta_{jkl}\underline{m}_j]^k\right. \\ &\left. + \sum_{\xi_k=1}^{k-1}[\zeta_{i\nu_k l}\underline{m}_i]^{\nu_k}\odot[\zeta_{j\xi_k l}\underline{m}_j]^{\xi_k}\right\}\end{aligned} \tag{3}$$

where $\nu_k = k - \xi_k$, $\underline{m}_i \odot \underline{m}_j = [m_{i_n} m_{j_n}]_{n=1,\ldots,N}$ and $\underline{m}_i^k = [m_{i_n}^k]_{n=1,\ldots,N}$. Further, (τ_1, τ_2) can be set to $(R-1, i+1)$ or (R, i). Moreover, $\zeta_{i\nu_k l}$, $\zeta_{i\xi_k l}$ and ϑ_{ikl} quantify the nonlinear effects provided by the ith endmember over the lth pixel within the kth order interactions. Finally, a_{rl} is the contribution to the linear mixture over the lth pixel provided by the rth endmember. Thus, as all the possible order-k ($k \le p$) interactions and interferences among pairs of endmembers can be provided by the model in (3), the aforesaid representation can be suited for reporting a thorough description of any p-linear mixtures. The model in (3) can be reduced to closed-form expression by properly setting the ϑ and ζ terms. Specifically, if we assume to set $p = 2$ and $\vartheta_{ikl} = 0\ \forall i$, (3) can be reduced as follows:

$$\underline{y}_l = \sum_{r=1}^{R} a_{rl}\underline{m}_r + \sum_{i=1}^{\tau_1}\sum_{j=\tau_2}^{R}\beta_{ijl}\underline{m}_i \odot \underline{m}_j \tag{4}$$

where $\zeta_{i1l}\cdot\zeta_{j1l} = \beta_{ijl}$. Thus, β_{ijl} is the coefficient that quantifies the second-order nonlinear effect of the product of endmembers $\underline{m}_i$ and $\underline{m}_j$ over the lth pixel. Moreover, (τ_1, τ_2) can be set to $(R-1, i+1)$ [16]–[18] or (R, i) [19] s.t. obtain different BMMs. Finally, the models in [16]–[18] differ along with the definition of the β terms and constraints.

On the other hand, in order to achieve a closed-form expression of an order-p nonlinear mixture model, we can assume to set the ϑ and ζ terms in (3) as follows:

$$\begin{aligned}\vartheta_{ikl} &= \left(\frac{\beta'_{ikl}}{R+1}\right)^{\frac{1}{k}} \\ \zeta_{iwl} &= (-1)^{\frac{\chi(w,\nu_k)}{\nu_k}}\cdot\left(\frac{\beta'_{ikl}}{R+1}\right)^{\frac{1}{k}}\cdot\binom{k}{\xi_k}^{\frac{1}{k}}\end{aligned} \tag{5}$$

where $w = \{\nu_k, \xi_k\}$ and $\chi(u, v) = 1 \leftrightarrow u = v$, while $\chi(u, v) = 0$ otherwise. Further, exploiting the binomial theorem according to

$$(a+b)^v = \sum_{u=0}^{v}\binom{v}{u}a^{v-u}b^u \tag{6}$$

the model in (3) can be rewritten as follows: if $(\tau_1, \tau_2) = (R, i)$:

$$\underline{y}_l = \sum_{r=1}^{R} a_{rl}\underline{m}_r + \sum_{k=2}^{p}\sum_{r=1}^{R}\beta'_{rkl}\underline{m}_r^k \tag{7}$$

where the overall contribution of the kth order delivered by the rth endmember over the lth pixel is driven by the coefficient β'_{rkl}. Hence, in order to be compliant with a coherent characterization of the endmembers' mix in the scene, the coefficients that drive the linear and nonlinear mixtures have to fulfill the following constraints:

$$\begin{gathered}a_{rl} \ge 0,\ \beta'_{rkl} \ge 0 \\ \sum_r a_{rl} + \sum_{rk}\beta'_{rkl} = 1 \\ \forall r \in \{1, \ldots, R\},\ k \in \{2, \ldots, p\}.\end{gathered} \tag{8}$$

As both the ϑ and ζ terms in (7) rely on the contribution of the β' parameters, it is not possible to obtain (4) from the aforementioned model. Therefore, the p-linear model that is proposed in this paper cannot be considered as an extension of (4). Indeed, the second-order mixture that can be drawn from (7) takes into account the nonlinear contributions provided by the interferences of endmembers [i.e., the terms that are driven by the ϑ coefficients in (3)], which are discarded by the BMMs as for (4).

The goal of p-linear spectral unmixing is to evaluate each a and β' term, in order to understand the nature of the endmember combination that delivers the given target pixel reflectance. It can be proved [11] that the coefficients driving the nonlinear combination in (7) can be obtained by means of a linear system involving the original hyperspectral data and the endmembers' spectra delivered by an EEA.

The method starts from considering $\underline{y}_l$ as the skeleton of a polytope with N vertices $\underline{v} = [v_i]_{i=1,\ldots,N}$, where each vertex is identified by a string of N coordinates, i.e., $v_i \Leftrightarrow (v_{i_k})_{k=1,\ldots,N}$ $\forall i \in \{1, \ldots, N\}$, being $v_{i_k} = y_{l_k}$ if $k = i$, 0 otherwise. Fig. 3 shows an $N = 3$-D instance of polytope skeleton.

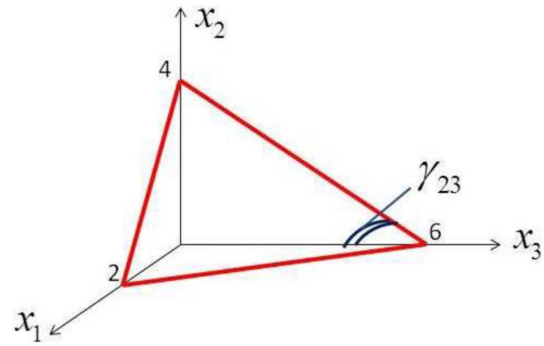

Fig. 3. Skeleton of a 3-D polytope identified by the spectral signature $\underline{y} = [2, 4, 6]$.

A convex polytope may be defined as an intersection of a finite number of half-spaces (H-representation) [20], [21]. That is, the affine space induced by the polytope is partitioned by $\binom{N}{2}$ hyperplanes that identify each of its facets. Thus, each hyperplane can be described by a linear inequality [20], [21] as follows:

$$\sum_{n=1}^{N} c_n x_n \le d \tag{9}$$

where x_n is the nth dimension in the N-dimensional space, being $n \in \{1, \ldots, N\}$. A closed convex polyhedron can be defined as the set of points that fulfill a system of linear inequalities such as $\sum_{n=1}^{N} c_{jn}x_{jn} \leq d_n$, where $j \in \{1, \ldots, (\frac{N}{2})\}$. Hence, the points on the edges of a polytope can be described by a linear system like $\underline{\underline{C}}\underline{x} = \underline{d}$. Specifically, the linear equation that can be drawn on the facet over the nth and mth dimension is as follows:

$$y_{l_m} + \tan(\gamma_{l_{mn}})y_{l_n} = 2y_{l_m} \tag{10}$$

where $\gamma_{l_{mn}}$ is the angle so that $\tan(\gamma_{l_{mn}}) = y_{l_m}/y_{l_n}$.

Thus, writing the aforementioned equation for each dimension pairs, it is possible to obtain a system of $M = (\frac{N}{2})$ linear equations. Therefore, the POD method aims at taking advantage of the overdetermination of the aforementioned system by exploiting the contribution of the a and β' terms in that. Specifically, applying proper algebraic properties to each possible dimension pairs, the following matrix equation is derived:

$$\underline{\underline{G}}_l\underline{\omega}_l = \underline{b}_l \tag{11}$$

where $\underline{\omega}_l = [\omega_l^{(j)}]_{j=1,\ldots,R}$, being $\omega_l^{(j)} = [\omega_{l_k}^{(j)}]_{k=1,\ldots,p}$, where $\omega_{l_k}^{(j)} = a_{jl}$ when $k = 1$, whereas $\omega_{l_k}^{(j)} = \beta'_{jkl}$ when $k > 1$. $\underline{\underline{G}}_l = [g_{l_{\kappa\lambda}}]$ is an $M \times Rp$ matrix, where $\kappa \in \{1, \ldots, M\}$ and $\lambda \in \{1, \ldots, Rp\}$, while $\underline{b}_l$ a vector of M elements. As previously mentioned, (11) is the core of the proposed POD method. Indeed, let us assume $\kappa = \rho_t + \eta_t$, where $t \in \{1, \ldots, N-1\}$, $\eta_t \in \{1, \ldots, N-t\}$, and $\rho_t = \sum_{u=1}^{t-1} N - u$ if $t > 1$, whereas $\rho_t = 0$ if $t = 1$. Then, in order to invert the model in (7), each element $g_{l_{\kappa\lambda}}$ must be defined as follows:

$$g_{l_{\kappa\lambda}} = g_{l_{(\rho_t+\eta_t),\lambda}} = m_{z_t}^{\psi_p} + \tan(\gamma_{l_{t,t+\eta_t}})m_{z_{t+\eta_t}}^{\psi_p} \tag{12}$$

where $\lambda = (z-1)p + \psi_p$, $z \in \{1, \ldots, R\}$, and $\psi_p \in \{1, \ldots, p\}$. Finally, $b_{l_\kappa} = b_{l_{(\rho_t+\eta_t)}} = 2y_{l_t}$.

Hence, the system in (11) represents a linear representation of the nonlinear mixture of each pixel according to the model in (7). Thus, the nonlinear HSU issue based on the p-linear model results in a linear programming problem that involves the original hyperspectral data and the endmembers' spectra according to the POD analysis [22]–[25]. Moreover, taking advantage of the thin QR factorization, the inversion process that aims at estimating the coefficients that drive the nonlinear mix is able to show a small condition number, s.t. the stability of the obtained solutions is preserved [26]. Further, each term in ω_l has to be compliant with the convex polytope representation, i.e., has to fulfill the constraints in (8).

At this point, it is important to note that the geometrical properties of the H-representation and the thin QR process guarantee that the sum-to-one constraint over the a and β terms in (7) is fulfilled, along with the nonnegativity constraint [21], [24], [25]. Further, it is possible to prove [27], [28] that the outcomes of the POD system approach more accurately the global optimum in inverting the mixture models, as the POD condition number is less than that delivered by other classic inversion algorithms such as fully constrained least square method [29]. Consequently, the POD method can deliver outputs that are more stable to perturbations in the mixing system, i.e., the reconstruction process can be enhanced and improved by the POD architecture.

However, there is still one point worth discussing. Since in our model, like in similar nonlinear models, nonlinear contributions to the abundances are not negligible, it is no more acceptable to set the abundances equal to the a coefficients. Indeed, this assumption may lead to a substantial performance degradation [9]. In [10], an abundance estimate metric that takes into account the second order nonlinear effects of each endmember has been proposed. Specifically, the aforesaid abundance computation relies on the assumption for which improved cover fraction estimates can be obtained by assigning the physically meaningless fraction to the physical ground components present in the pixel. Hence, in bilinear mixture scenarios, the pixel distribution factor of every endmember can be optimally estimated by the component's ground cover fraction, leading to a compact form for abundance estimations [10].

However, in case of p-linear mixing when $p > 2$, this property might not hold, as the complex geometry of the given IFOV can affect the pixel distribution factor evaluation. Indeed, the multiple scatterings that can be characterized by p-linear mixture models can occur in case of multiple layers and interactions among endmembers. Thus, the pixel distribution of each element that shows up in a given scene can result from complex processes of interplays which might be hardly described by a linear relationship as in [10]. Therefore, in order to accurately evaluate the abundances in higher order mixtures scenes, here an aggregate metric based on the polytope H-representation is proposed.

To this aim, let us write the reconstructed pixel $\underline{\hat{y}}_l$ as

$$\hat{y}_{l_n} = \sum_{r=1}^{R} \varphi_{rl_n} m_{r_n} = \sum_{r=1}^{R}\sum_{k=1}^{p} \omega_{l_k}^{(r)} m_{r_n}^k \tag{13}$$

where φ_{rl_n} is the overall contribution of the rth endmember to the reconstruction of the lth pixel over the nth band. Geometrically speaking, it is possible to think of φ_{rl_n} as the compression/expansion factor of the rth endmember over the nth direction in the N-dimensional space. As the relevance of the rth endmember in contributing to the reconstruction of the lth pixel increases, the amplitude of $\underline{\varphi}_{rl} = [\varphi_{rl_n}]_{n=1,\ldots,N}$ gets larger as well. Thus, in order to quantify the contribution of each endmember to the reconstruction of the lth pixel, let us consider the polytope that is induced by the vertices identified by $\underline{\varphi}_{rl}$. Given our assumptions such a polytope is a simplex [20]. Therefore, we can define its volume $V_{\underline{\varphi}_{rl}}$ using the formula

$$V_{\underline{\Gamma}} = \frac{1}{N!}\det[\Delta(\underline{\Gamma})] = \frac{1}{N!}\prod_{n=1}^{N}\Gamma_n \tag{14}$$

where $\Delta(\underline{\Gamma}) = [\delta_{ij}(\underline{\Gamma})]_{(i,j)\in\{1,\ldots,N\}^2}$ is the diagonal matrix induced by the $\underline{\Gamma} = [\Gamma_n]_{n=1,\ldots,N}$ spectral signature [20]. That is, $\delta_{ij}(\underline{\Gamma}) = \Gamma_n \leftrightarrow i = j = n$, whereas $\delta_{ij}(\underline{\Gamma}) = 0$ otherwise. Hence, the proposed estimated rth endmember abundance $\hat{a}_{rl}$ can be defined as

$$\hat{a}_{rl} = \frac{V_{\underline{\varphi}_{rl}}}{\sum_{i=1}^{R} V_{\underline{\varphi}_{il}}}. \tag{15}$$

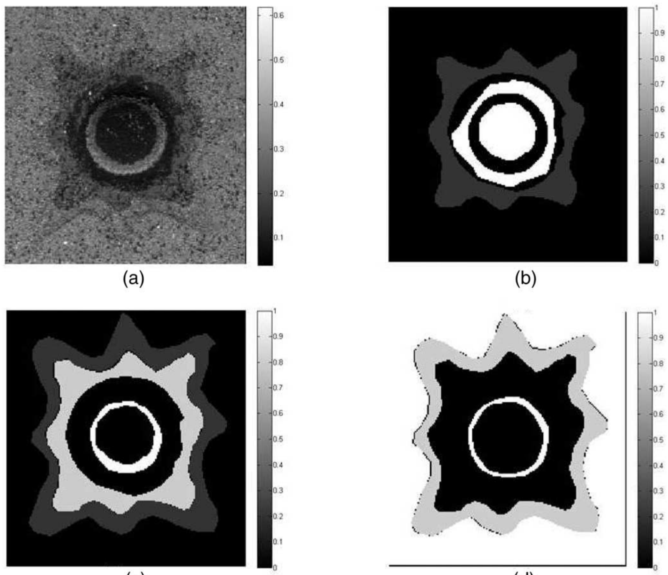

Fig. 4. (a) Original reflectance distribution in the crater scene on the 16th band. Each endmember is distributed according to the reported abundance maps. (b) Basalt. (c) Palagonite. (d) Tephra.

It should be noted that the abundance estimates in (15) fulfill the sum-to-one and the nonnegativity constraints [9].

III. Experimental Results

In this section, we will focus on showing the capacity of the proposed methodology. A thorough comparison of nonlinear unmixing algorithms [9] is beyond the scope of this paper. We first tested the performance of the aforementioned methods over a target that has been artificially generated in [30]. Specifically, the authors in [30] provide a simulation of a crater obtained by modifying a martian regolith. This target shows a complex photometric behavior because of its digital elevation model (DEM) and the Hapke's model-based mixture of the composing minerals (i.e., basalt, palagonite, and tephra). The target scene is composed by 186×174 pixels. 16 bands in a wavelength range from 400 nm to 1100 nm have been considered. Fig. 4(a) shows the reflectance map of the aforementioned scene over the 16th band. Further, the abundance maps of basalt, palagonite, and tephra are reported in Fig. 4(b), (c), and (d), respectively.

In [30], the authors deliver several methods to unmix the aforementioned image by deconvoluting the mixing process. These algorithms differ in the available quantitative information of the target they use to perform the unmixing process. Specifically, given the bidirectional reflectance image, they can consider conversion in single scattering albedo, information on incidence and emergence angles, material properties, and surface macroscopic roughness in a pixel. On the other hand, POD is used to unmix the bidirectional reflectance image by considering the endmembers' reflectance spectra provided in [30]. It is worth noting that no other information but the target and the endmembers' reflectance spectra are available for POD.

We compared the unmixing performance by computing the mean absolute difference of the mineralogical fraction images

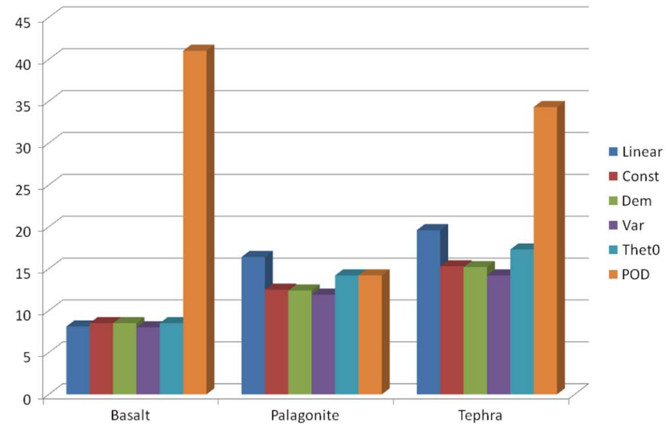

Fig. 5. Percentage of mean absolute difference of the MFIs for each endmember in the crater scene. The considered methods are POD and those provided in [30].

(MFIs) [30] for each endmember. Then, we computed the percentage of mean absolute difference between calculated MFI and ideal MFI for each algorithm. Fig. 5 reports the aforesaid quantity for POD and those provided in [30]. The nonlinearity order p in POD has been set to 3. Apparently, POD delivers very poor performance in reconstructing the crater scene. One of the main reasons for this result lies in the mismatch between the Hapke's model and the polynomial approximation implied by POD method. Since POD is unable to efficiently track the nonlinearity induced by the bidirectional reflectance model, the reconstruction can be dramatically degraded. Moreover, it is worth noting that the linear estimation of the abundance maps from an image that has been not very efficiently nonlinearly reconstructed can further jeopardize the MFI evaluation as well.

We tested the new architecture over an image acquired over the World Trade Center area in New York City [Fig. 6(a)], collected by the AVIRIS instrument on September 16, 2001, just 5 days after the terrorist attacks that collapsed the two main towers and other buildings in the WTC area. The full data set considered consists on 614×507 pixels, with $N = 224$ bands and a spatial resolution of 1.7 m/pixel. Fig. 6(a) shows a false color composite of the area using the 1.682, 1.107, and 655 nm channels, displayed as red, green, and blue respectively. Extensive reference information, collected by the U.S. Geological Survey (USGS), is available for the WTC scene. The endmembers of the WTC scene have been extracted using OSP algorithm [31], which provided the reflectance spectra of ten endmembers used to feed the architecture in Fig. 2.

We have used the ANN to estimate the nonlinearity order of each pixel, randomly generating 8000 samples as training set. The aforesaid endmembers have been considered to feed the POD method [11]. Specifically, ANN marked 63.9% of the pixels in the scene to show nonlinearities of the fifth order, 35.5% of the pixels have been labeled as driven by linear mixture. Finally, 0.1% and 0.5% of the pixels have been estimated to show nonlinearities of the second and third order, respectively. When employing the POD method only to unmix the scene, the order of nonlinearity p for each pixel has been set to 5, which is the maximum nonlinearity order estimated by ANN.

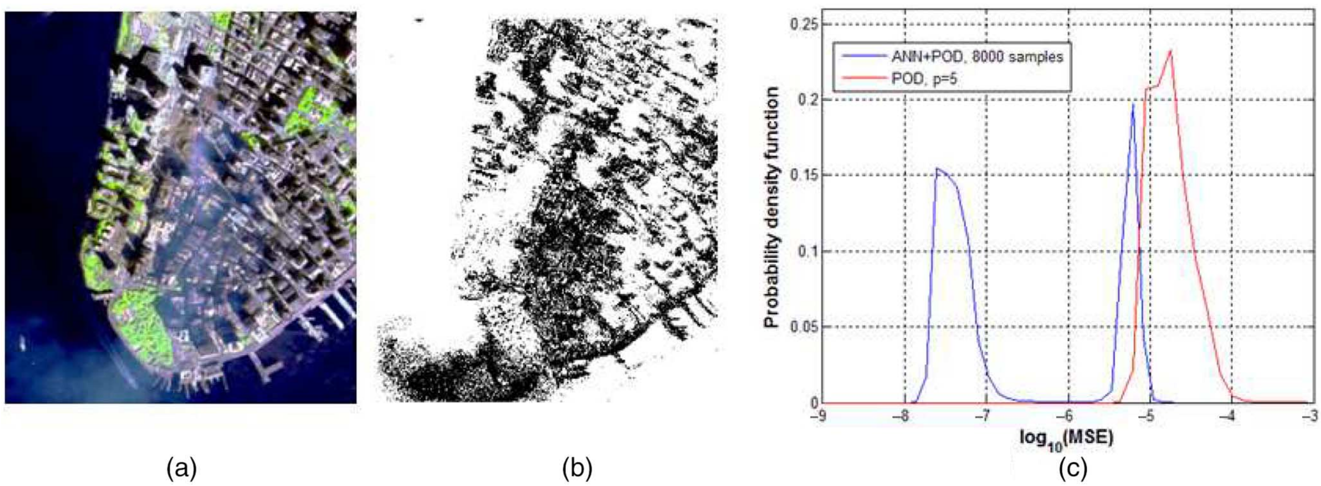

Fig. 6. (a) False color composition of AVIRIS hyperspectral image collected by the NASA's Jet Propulsion Laboratory over lower Manhattan on September 16, 2001. (b) Distribution of the pixels over which the architecture in Fig. 2, where 8000 samples have been used as training set delivers an RE improvement over the RE provided by POD method with $p = 5$. (c) Probability density function of the mean-square error obtained over the WTC image by means of the architecture in Fig. 2, when 8000 samples are used as training sets (blue line) and of the POD method when the nonlinearity order has been set to 5 for each pixel (red line). Ten endmembers have been extracted using OSP algorithm.

We can summarize the reconstruction performance of the considered unmixing methods by means of the so-called RE which can be defined (for an image composed by P pixels and with N bands) as

$$RE = \sqrt{\frac{1}{PN}\sum_{l=1}^{P} \|\underline{y}_l - \hat{\underline{y}}_l\|^2} \tag{16}$$

where, according to (13), $\hat{\underline{y}}_l$ is the the reconstructed spectral signature.

Figs. 6 and 7 summarize the results in terms of RE that have been achieved. Apparently, the proposed architecture outperforms the POD method. Indeed, the use of ANN to estimate the nonlinearity order provides an RE while $RE = 1.5 \cdot 10^{-3}$ using 8000 samples as training set. On the other hand, the POD method with $p = 5$ for each pixel only delivers $RE = 4.6 \cdot 10^{-3}$ (Fig. 7). The probability density function of the mean-square error provided by the architecture in Fig. 2, where 8000 samples are used as training sets and by POD when $p = 5$ is reported in Fig. 6(c).

It is possible to appreciate the improvement delivered by the careful estimation of the nonlinearity order as provided by ANN taking a look at Fig. 6(c) and(b), where the pixels for which the RE obtained by using the architecture in Fig. 2, where 8000 samples have been used as training set is less than that achieved by the POD method are shown. Hence, Fig. 6(b) gives a figure of the overfitting distribution over the World Trade Center scene.

We also tested the performance of the methods in Section II over a real image recorded over the Istanbul area by Hyperion in 2001 [Fig. 8(a)]. The scene is composed by 400×400 pixels. 198 calibrated bands in a wavelength range spanning from 426.82 to 2395.5 nm have been considered. We can summarize the reconstruction performance of the considered unmixing methods method by means of RE and the abundance estimates delivered according to (15).

Fig. 7. RE obtained over the World Trade Center scene using POD when the order of the considered nonlinearity p is set to 5 and the proposed architecture (ANN + POD) when the number of samples to build up the training set is set to 8000. Ten endmembers have been extracted using OSP algorithm.

Fig. 9 reports the RE performance delivered by three unmixing methods: 1) fully constrained least-squares unmixing (FCLSU) [29]; 2) ANN; and 3) POD. These algorithms have been fed with the reflectance spectra of ten endmembers that have been extracted by means of orthogonal subspace projection (OSP) [32]. Further, POD is performed when the nonlinearity order p is set to 3 and 4. Apparently, POD outperforms both the other methods. Specifically, POD reaches $RE = 1.2 \cdot 10^{-3}$ when $p = 4$, while ANN's RE is about 0.035. This behavior is the result of the lack of ground truth information at subpixel level over the Istanbul scene apart from the endmembers obtained by the EEA. Thus, ANN is not able to properly train its network in order to achieve a good approximation of the nonlinear mixing process.

Further, we tested the performance in terms of RE of the combined ANN-POD architecture shown in Fig. 2. Again, ten endmembers were extracted using the OSP algorithm. ANN

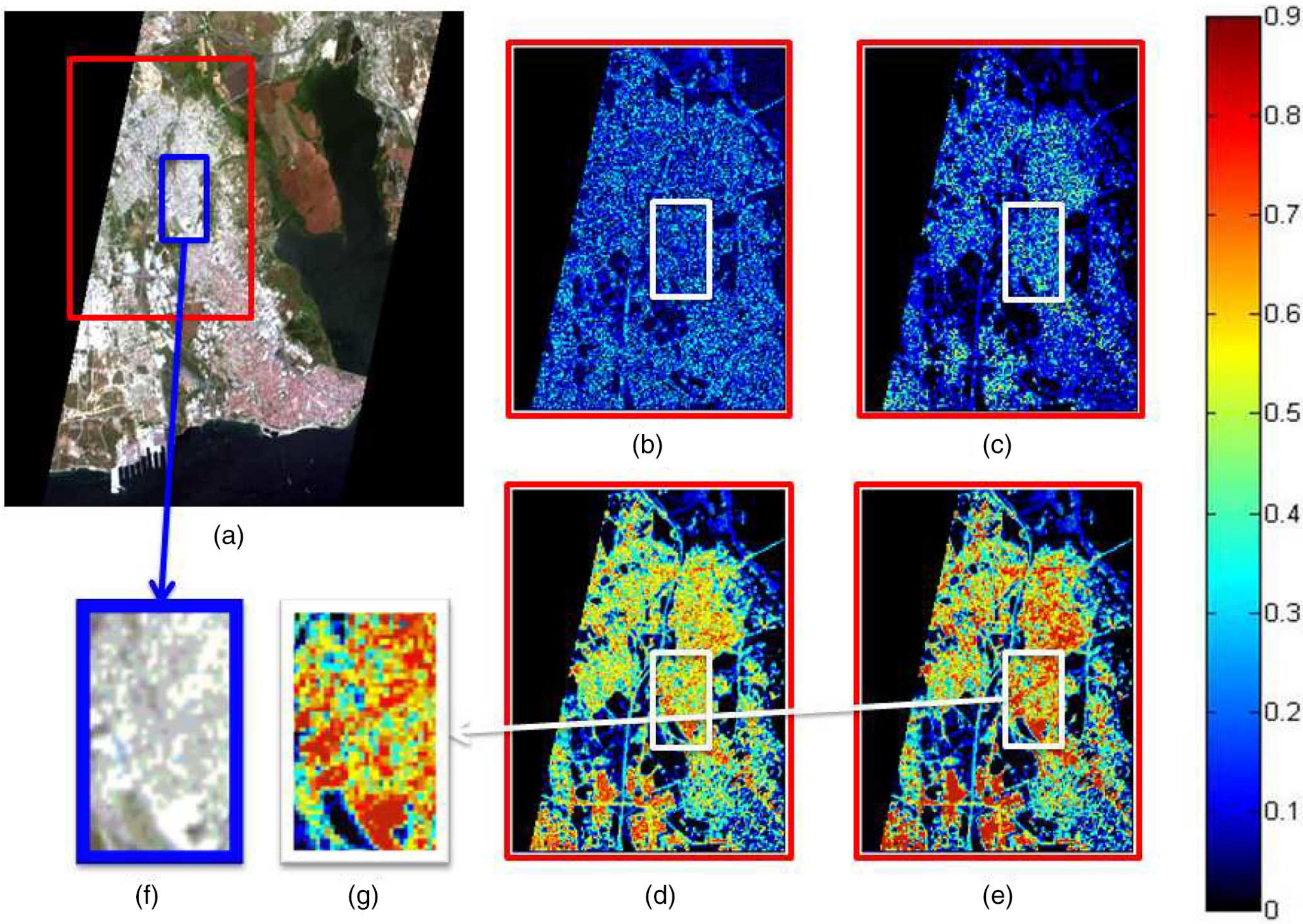

Fig. 8. (a) False color composition of Hyperion hyperspectral image collected over Istanbul. The abundance of the endmember associated with the urban extents in the red box in (a) have been estimated by means of HSU based on (b) LMM, (c) BMM as in [19], (d) POD when $p = 5$, and (e) POD when the nonlinearity orders have been estimated by ANN. Finally, (f) depicts a small sample of the original data, while (g) shows the results for the same area, here shown to appreciate the fine level of details that the new approach is able to reach.

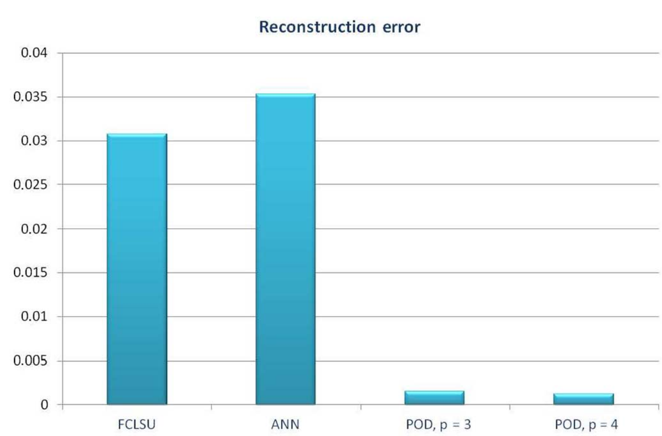

Fig. 9. RE obtained over the Istanbul scene using fully constrained least-squares unmixing (FCLSU), ANN and POD when the order of the considered nonlinearity p is set to 3 and 4. 10 endmembers have been extracted using orthogonal subspace projection (OSP).

estimates the maximum order of polynomial nonlinearity for every pixel in the scene. Then, this information is delivered to POD algorithm together with the endmembers' spectra. In this context, POD algorithm is performed over each pixel by setting the nonlinearity order p to the corresponding estimated order provided by ANN. Specifically, ANN marked 60.1% of the pixels in the scene to show nonlinearities of the fifth order, 35.7% of the pixels have been labeled as driven by linear mixture. Finally, 0.5%, 1.4%, and 2.3% of the pixels have been estimated to show nonlinearities of the second, third, and fourth order, respectively.

Fig. 10 shows the RE performance for the new ANN-POD architecture introduced in this work. Specifically, the blue solid line represents the RE achieved using ANN followed by POD as a function of the number of samples that have been used for training. The estimation of the nonlinearity order has been repeated 10 times for each case combining the results by majority voting. It is not surprising that the RE performance improves as the number of training samples increases. Moreover, the dashed lines identify the REs that have been achieved when only POD is used, setting the nonlinearity order p to 3 (green line), 4 (red line), and 5 (black line) for each pixel in the scene. Comparing these results to the RE curve, we got from the combination of ANN and POD, we can see that the number of training samples plays a key role in providing good reconstruction performance. In fact, the proposed framework outperforms POD when 4000 samples are used to train the ANN. Thus,

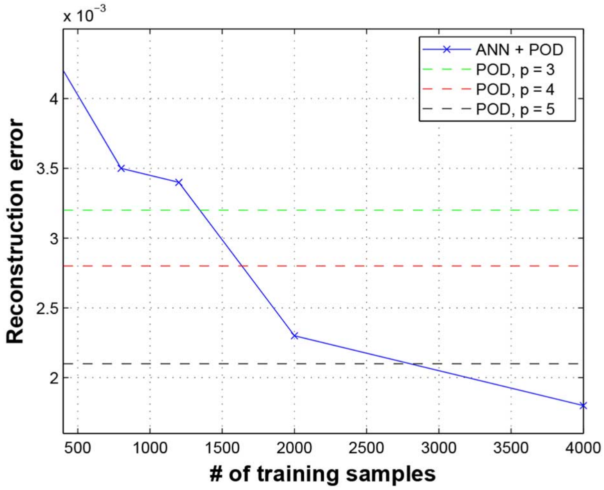

Fig. 10. RE for the Istanbul scene as a function of the number of training samples that have been used by the ANN to estimate the nonlinearity order p of each pixel (blue solid line). The dashed green, red and black lines identify the RE that has been obtained using POD when p has been set for every pixel to 3, 4 and 5, respectively.

TABLE I
AVERAGE EXECUTION TIMES (IN SECONDS) FOR THE ESTIMATION OF THE NONLINEARITY WHEN USING 400, 800, 1200, 2000, AND 4000 TRAINING PATTERNS

	Number of training patterns				
	400	800	1200	2000	4000
Avg. training time (s)	960.75	995.99	1205.31	1360.17	3812.95

apparently, the estimation of the nonlinearity order by ANN is delivering actual reconstruction results as the training is performed over a larger amount of pixels. It should be noticed that we synthetically generate the training samples, thus the availability of ground-truth information is not a problem.

Further analysis is needed in order to determine an optimal methodology to estimate the nonlinearity orders (sufficient number of artificially generated training samples, supervised/semisupervised nonlinear classifier, etc.). Computational complexity of this step is severe. We report execution times of the nonlinear estimation step over a 1.7-GHz Intel Core I5 with 4 GB 1333 MHz DDR3 (see Table I). Although the system is not a last generation computer, additional analysis must be accomplished beyond this proof of concept in order to accelerate this step. For the sake of completeness, we have analyzed the variance of the randomly generated high-order interactions between endmembers and compare it with the variance of zero mean Gaussian noise [32] in different signal-to-noise ratios (SNRs) from 10:1 to 1000:1. Actually, we generate 10 000 training samples with random coefficients and nonlinearity orders within [1,10] (1000 training samples for each order) using the five endmembers provided by OSP. The variance of randomly generated interactions between endmembers is in the order of 10^{-3} for all considered nonlinearity orders, while in the case of the lower SNR considered (10:1), the variance is in the order of 10^{-6}, thus the variance in high order scattering effects is more significative than in noise effects.

Finally, we tested the abundance estimation over the Istanbul scene using LMM, BMM in [19], POD when $p = 5$ and when the nonlinearity orders are estimated through ANN with 8000 samples used as training set. Fig. 8(b)–(e) shows the aforementioned results over the detail in the red box in Fig. 8(a), respectively. Apparently, higher order HSU strongly outperforms linear and bilinear unmixing. Further, it is possible to state that the combined ANN-POD framework outperforms POD when $p = 5$, s.t. evaluation of the abundance for the endmember which identifies the urban extents is enhanced by proper estimate of the nonlinearity orders.

These effects are even more apparent by comparing the detail in Fig. 8(f) to the abundance estimated by the architecture in Fig. 2 over the same area of Fig. 8(a). Indeed, Fig. 8(g) shows how the combined ANN-POD framework is able to precisely characterize the urban extents Further, the abundance estimates performed by POD and combined ANN-POD framework are much more detailed and highlighted than those computed by linear and bilinear HSU. Thus, higher order nonlinearities over the Istanbul scene deliver strong contribution to the the spectral mixture that has been recorded by Hyperion sensor. Indeed, higher order nonlinear effects can play a key role especially in very complex scenes, where several endmembers interplay and where a large amount of scattering comes across the sensor. Hence, as urban scenes can be strongly affected by the aforementioned effects [33], the unmixing gain provided by architectures that rely on the proposed p-linear model can be very relevant, as shown in Fig. 8.

IV. Conclusion and Future Lines

In this paper, we have developed a new method for nonlinear spectral unmixing which combines ANNs and POD. The ANN is used to estimate the order of the nonlinearity involved in the problem, while POD is used to perform the actual unmixing. Our experimental results with both simulated and real hyperspectral data sets show promising results. Future work will focus on testing the proposed framework in different scenarios, in order to evaluate its capacity to provide effective solutions using limited or no prior information, optimizing the nonlinearity estimation step, reducing the amount of necessary training patterns, and improving its computational complexity.

Acknowledgment

The authors would like to thank Sylvain Douté (IPAG-Grenoble) for providing the martian crater image. The authors would also like to thank NASA Jet Propulsion Laboratory for the use of AVIRIS World Trade Center data. Last, but not least, the authors acknowledge the anonymous reviewers and the editors for their comments and suggestions which greatly helped to improve the technical quality and presentation of this paper.

REFERENCES

[1] M. Faber, N. Niemes, and G. Stephan, *Entropy, Environment and Resources*, 2nd ed. Berlin, Germany: Springer-Verlag, 1995.

[2] A. Marinoni and P. Gamba, "Big data for human-environment interaction assessment: Challenges and opportunities," in *Proc. ESA Big Data Space Conf. (BiDS)*, Frascati, Italy, Nov. 2014, pp. 1–4.

[3] D. Pimentel *et al.*, "Environmental and economic costs of soil erosion and conservation benefits," *Science*, vol. 267, pp. 1117–1123, Feb. 1995.

[4] J. M. Bioucas-Dias *et al.*, "Hyperspectral unmixing overview: Geometrical, statistical, and sparse regression-based approaches," *IEEE J. Sel. Topics Appl. Earth Observ. Remote Sens.*, vol. 5, no. 2, pp. 354–379, Apr. 2012.

[5] J. Plaza, A. Plaza, R. Perez, and P. Martinez, "On the use of small training sets for neural network-based characterization of mixed pixels in remotely sensed hyperspectral images," *Pattern Recognit.*, vol. 42, pp. 3032–3045, 2009.

[6] J. Chen, C. Richard, and P. Honeine, "Nonlinear unmixing of hyperspectral data based on a linear-mixture/nonlinear-fluctuation model," *IEEE Trans. Signal Process.*, vol. 61, no. 2, pp. 480–492, Jan. 2013.

[7] N. Dobigeon *et al.*, "Nonlinear unmixing of hyperspectral images: Models and algorithms," *IEEE Signal Process. Lett.*, vol. 31, no. 1, pp. 82–94, Jan. 2014.

[8] Y. Altmann, A. Halimi, N. Dobigeon, and J.-Y. Tourneret, "Supervised nonlinear spectral unmixing using a postnonlinear mixing model for hyperspectral imagery," *IEEE Trans. Image Process.*, vol. 21, no. 6, pp. 3017–3025, Jun. 2012.

[9] R. Heylen, M. Parente, and P. Gader, "A review of nonlinear hyperspectral unmixing methods," *IEEE J. Sel. Topics Appl. Earth Observ. Remote Sens.*, vol. 7, no. 6, pp. 1844–1868, Jun. 2014.

[10] B. Somers *et al.*, "Nonlinear hyperspectral mixture analysis for tree cover estimates in orchards," *Remote Sens. Environ.*, vol. 113, no. 6, pp. 1183–1193, Jun. 2009.

[11] A. Marinoni and P. Gamba, "Non-linear hyperspectral unmixing by polytope decomposition," in *Proc. IEEE Workshop Hyperspectral Image Signal Process. Evol. Remote Sens. (WHISPERS)*, Lausanne, Switzerland, Jun. 2014, pp. 1–4.

[12] W. Liu and E. Y. Wu, "Comparison of nonlinear mixture models: Sub-pixel classification," *Remote Sens. Environ.*, vol. 94, pp. 145–154, 2005.

[13] J. Plaza and A. Plaza, "Spectral mixture analysis of hyperspectral scenes using intelligently selected training samples," *IEEE Geosci. Remote Sens. Lett.*, vol. 7, no. 2, pp. 371–375, Apr. 2010.

[14] J. Plaza, R. Perez, P. Martinez, and A. Plaza, "Joint linear/nonlinear spectral unmixing of hyperspectral image data," in *Proc. IEEE Int. Geosci. Remote Sens. Symp.*, Barcelona, Spain, Jul. 2007, pp. 4037–4040.

[15] G. Hughes, "On the mean accuracy of statistical pattern recognizers," *IEEE Trans. Inf. Theory*, vol. 14, no. 1, pp. 55–63, Jan. 1968.

[16] J. M. P. Nascimento and J. M. Bioucas-Dias, "Nonlinear mixture model for hyperspectral unmixing," *Proc. SPIE Image Signal Process. Remote Sens. XV*, vol. 7447, no. 1, p. 744701, 2009.

[17] W. Fan, B. Hu, J. Miller, and M. Li, "Comparative study between a new nonlinear model and common linear model for analysing laboratory simulated-forest hyperspectral data," *Int. J. Remote Sens.*, vol. 30, no. 11, pp. 2951–2962, Jun. 2009.

[18] A. Halimi, Y. Altmann, N. Dobigeon, and J.-Y. Tourneret, "Nonlinear unmixing of hyperspectral images using a generalized bilinear model," *IEEE Trans. Geosci. Remote Sens.*, vol. 49, no. 11, pp. 4153–4162, Nov. 2011.

[19] I. Meganem, P. Deliot, X. Briottet, Y. Deville, and S. Hosseini, "Linear-quadratic mixing model for reflectances in urban environments," *IEEE Trans. Geosci. Remote Sens.*, vol. 52, no. 1, pp. 544–558, Jan. 2014.

[20] B. Grunbaum, *Convex Polytopes*, 2nd ed. Berlin, Germany: Springer-Verlag, 2003.

[21] G. H. Golub and C. F. Van Loan, *Matrix Computations*, 3rd ed. Baltimore, MD, USA: The Johns Hopkins Univ. Press, 1996.

[22] I. N. Herstein, *Topics in Algebra*, 2nd ed. Hoboken, NJ, USA: Wiley, 1975.

[23] V. V. Prasolov, *Problems and Theorems in Linear Algebra*. Providence, RI, USA: American Mathematical Society, 1991.

[24] G. E. Bredon, *Topology and Geometry*. Berlin, Germany: Springer-Verlag, 1993.

[25] V. Kaibel and A. Schwartz, "On the complexity of polytope isomorphism problems," *Graphs Comb.*, vol. 19, no. 2, pp. 215–230, 2003.

[26] W. Cheney and D. Kincaid, *Numerical Mathematics and Computing*, 6th ed. Boston, MA, USA: Thomson Learning, Inc. 2008.

[27] L. N. Trefethen and D. Bau, *Numerical Linear Algebra*. Philadelphia, PA, USA: SIAM, 1997.

[28] A. Marinoni and P. Gamba, "A novel approach for efficient p-linear hyperspectral unmixing," *IEEE J. Sel. Topics Signal Process.*, 2015, vol. 9, no. 6, Sep. 2015.

[29] D. Heinz and C.-I. Chang, "Fully constrained least squares linear spectral mixture analysis method for material quantification in hyperspectral imagery," *IEEE Trans. Geosci. Remote Sens.*, vol. 39, no. 3, pp. 529–545, Mar. 2001.

[30] A. M. Cord, P. C. Pinet, Y. Daydou, and S. D. Chevrel, "Experimental determination of the surface photometric contribution in the spectral reflectance deconvolution processes for a simulated martian crater-like regolitic target," *Icarus*, vol. 175, no. 1, pp. 78–95, Aug. 2004.

[31] H. Ren and C.-I Chang, "Automatic spectral target recognition in hyperspectral imagery," *IEEE Trans. Aerosp. Electron. Syst.*, vol. 39, no. 4, pp. 1232–1249, Oct. 2003.

[32] J. C. Harsanyi and C.-I. Chang, "Hyperspectral image classification and dimensionality reduction: An orthogonal subspace projection," *IEEE Trans. Geosci. Remote Sens.*, vol. 32, no. 4, pp. 779–785, Jul. 1994.

[33] A. Marinoni and P. Gamba, "On the effect of nonlinear mixing in hyperspectral images of human settlements," in *Proc. Joint Urban Remote Sens. Event (JURSE)*, Lausanne, Switzerland, Mar. 2015, pp. 1–4.

Andrea Marinoni (S'07–M'11) received the B.Sc., M.Sc. (*cum laude*), and Ph.D. degrees in electronic engineering from the University of Pavia, Pavia, Italy, in 2005, 2007 and 2011, respectively.

Since 2011, he has been a Postdoctoral Fellow with the Telecommunications and Remote Sensing Laboratory, Department of Electrical, Computer, and Biomedical Engineering, University of Pavia. In 2009, he has been a Visiting Researcher at the University of California, Los Angeles (UCLA), Los Angeles, CA, USA. His research interests include efficient nonlinear signal processing applied to hyperspectral unmixing, astroinformatics and Big Data mining, analysis, and management for human–environment interaction assessment.

Dr. Marinoni has been an Invited Speaker at 2010 Workshop on Application of Communication Theory to Emerging Memory Technologies, IEEE Global Communications conference (GLOBECOM), Miami, FL, 2014 New Challenges in Astro- and Environmental Informatics in the Big Data Era Workshop, Szombathely, Hungary, and Big Data Methodologies in Remote Sensing and Astronomy special session at 2015 IEEE Geoscience and Remote Sensing Symposium, Milan, Italy. In 2011, he has been the recipient of the two-year "Dote Ricerca Applicata" Award, sponsored by the Region of Lumbardy, Italy, and STMicroelectronics N.V.

Javier Plaza (M'09) was born in Caceres, Spain, in 1979. He received the Bachelor's degree in 2002, the M.Sc. degree in 2004, and the Ph.D. degree in 2008, all in computer engineering, from the University of Extremadura, Cáceres, Spain.

He is currently an Associate Professor with the Department of Technology of Computers and Communications, University of Extremadura. He has authored or coauthored more than 100 scientific publications including more 30 journal citation report papers, book chapters, and peer-reviewed conference proceedings. His research interests include remotely sensed hyperspectral imaging, pattern recognition, signal and image processing, neural networks and efficient implementation of large-scale scientific problems on parallel and distributed computer architectures.

Dr. Plaza has served as a Reviewer for more than 150 papers submitted to more than 25 different journals, including the IEEE TRANSACTIONS ON GEOSCIENCE AND REMOTE SENSING, IEEE JOURNAL OF SELECTED TOPICS IN APPLIED EARTH OBSERVATIONS AND REMOTE SENSING, IEEE GEOSCIENCE AND REMOTE SENSING LETTERS, IEEE TRANSACTIONS ON IMAGE PROCESSING, IEEE TRANSACTIONS ON SIGNAL PROCESSING, IEEE JOURNAL OF SELECTED TOPICS IN SIGNAL PROCESSING, AND IEEE TRANSACTIONS ON SYSTEMS, MAN, AND CYBERNETICS C. He was the recipient of the Outstanding Ph.D. Dissertation Award at the University of Extremadura in 2008.

Antonio Plaza (M'05–SM'07–F'15) was born in Cáceres, Spain, in 1975.

He is an Associate Professor (with accreditation for Full Professor) with the Department of Technology of Computers and Communications, University of Extremadura, Cáceres, Spain, where he is the Head of the Hyperspectral Computing Laboratory (HyperComp). His research interests include hyperspectral data processing and parallel computing of remote sensing data. He has been the advisor of 12 PhD dissertations and more than 30 MsC dissertations. He was the Coordinator of the Hyperspectral Imaging Network, a European project with total funding of 2.8 million Euro. He has reviewed more than 500 manuscripts for over 50 different journals. He has authored more than 400 publications, including 142 journal papers (92 in IEEE journals), 20 book chapters, and over 240 peer-reviewed conference proceeding papers (94 in IEEE conferences). He has edited a book on *High-Performance Computing in Remote Sensing* (CRC Press/Taylor & Francis) and guest edited 8 special issues on hyperspectral remote sensing for different journals.

Dr. Plaza served as the Director of Education Activities for the IEEE Geoscience and Remote Sensing Society (GRSS) in 2011–2012, and is currently serving as President of the Spanish Chapter of IEEE GRSS (since November 2012). He is currently serving as the Editor-in-Chief of the IEEE TRANSACTIONS ON GEOSCIENCE AND REMOTE SENSING. He has served as a Proposal Evaluator for the European Commission, the National Science Foundation, the European Space Agency, the Belgium Science Policy, the Israel Science Foundation, and the Spanish Ministry of Science and Innovation. He is a recipient of the recognition of Best Reviewers of the IEEE GEOSCIENCE AND REMOTE SENSING LETTERS in 2009 and the IEEE TRANSACTIONS ON GEOSCIENCE AND REMOTE SENSING in 2010, a journal for which he served as Associate Editor in 2007–2012. He is also an Associate Editor for IEEE ACCESS, and was a member of the Editorial Board of the IEEE GEOSCIENCE AND REMOTE SENSING NEWSLETTER (2011–2012) and the IEEE GEOSCIENCE AND REMOTE SENSING MAGAZINE (2013). He was also a member of the steering committee of the IEEE JOURNAL OF SELECTED TOPICS IN APPLIED EARTH OBSERVATIONS AND REMOTE SENSING (JSTARS). He is a recipient of the 2013 Best Paper Award of the JSTARS journal, and a recipient of the most highly cited paper (2005–2010) in the *Journal of Parallel and Distributed Computing*. He received the Best Paper Awards at the IEEE International Conference on Space Technology and the IEEE Symposium on Signal Processing and Information Technology. He is a recipient of the Best Ph.D. Dissertation Award at the University of Extremadura, a recognition also received by five of his Ph.D. students.

Paolo Gamba (SM'00–F'13) received the Laurea degree (*cum laude*) and the Ph.D. degree in electronic engineering from the University of Pavia, Pavia, Italy, in 1989 and 1993, respectively.

He is an Associate Professor of Telecommunications with the University of Pavia, where he also leads the Telecommunications and Remote Sensing Laboratory. He has been invited to give keynote lectures and tutorials in several occasions about urban remote sensing, data fusion, EO data and risk management. He has authored more than 110 papers in international peer-review journals and presented more than 250 research works in workshops and conferences.

Dr. Gamba served as Editor-in-Chief of the IEEE GEOSCIENCE AND REMOTE SENSING LETTERS from 2009 to 2013, and as Chair of the Data Fusion Committee of the IEEE Geoscience and Remote Sensing Society from October 2005 to May 2009. Currently, he is the Chair of the Chapters Committee of the same society. He has been the Organizer and Technical Chair of the biennial GRSS/ISPRS Joint Workshops on "Remote Sensing and Data Fusion over Urban Areas" since 2001. He also served as Technical Co-Chair of the 2010 IEEE Geoscience and Remote Sensing Symposium, Honolulu, Hawaii, July 2010, and Technical Co-Chair of the 2015 IEEE Geoscience and Remote Sensing Symposium, in Milan, Italy. He has been the Guest Editor of special issues of the IEEE TRANSACTIONS ON GEOSCIENCE AND REMOTE SENSING, IEEE JOURNAL OF SELECTED TOPICS IN REMOTE SENSING APPLICATIONS, *ISPRS Journal of Photogrammetry and Remote Sensing*, *International Journal of Information Fusion and Pattern Recognition Letters* on the topics of urban remote sensing, remote sensing for disaster management, and *Pattern Recognition in Remote Sensing Applications*.